*J. Fluid Mech.* (2009), *vol.* 629, *pp.* 425–443.  
doi:10.1017/S0022112009006521 Printed in the United Kingdom

# Flow of a viscous incompressible fluid after a sudden point impulse near a wall

B. U. FELDERHOF†

Institut für Theoretische Physik A, RWTH Aachen University, Templergraben 55, 52056 Aachen, Germany

(Received 5 December 2008 and in revised form 9 February 2009)

The flow of a viscous incompressible fluid generated by a sudden impulse near a wall with no-slip boundary condition is studied on the basis of the linearized Navier–Stokes equations. It turns out that the flow differs significantly from that for the perfect slip boundary condition, except far from the wall and at short times. At short time the flow is irrotational and can be described by a potential which varies with the square root of time. Correspondingly the pressure disturbance is quite large at short times. It shows an oscillation at later times if the impulse is directed parallel to the wall and decays monotonically for impulse perpendicular to the wall.

## 1. Introduction

If a viscous fluid, which is initially at rest, is set in motion by a sudden small impulse at a point, it quickly develops a flow extending over large distances (Lighthill 1986). In the limit in which the fluid is incompressible, with hydrodynamics described by the linearized Navier–Stokes equations, the flow at short time is irrotational and may be derived from a potential which depends strongly on the shape of the container. The flow at later times is affected significantly by the boundary condition imposed at the wall of the container. In the following we study the time-dependent motion for a half-space bounded by a plane wall with either a perfect slip or a no-slip boundary condition.

The analysis amounts to a study of the Green function of the linearized Navier–Stokes equations for the geometry under consideration. For the perfect slip boundary condition the Green function, as a function of spatial coordinates and time, is derived easily from that for infinite space by the method of images (Pagonabarraga *et al.* 1998; Frydel & Rice 2007). For the no-slip boundary condition the Green function is much more complicated. In earlier work it has been calculated as a Fourier transform with respect to the Cartesian coordinates parallel to the wall and with respect to time (Jones 1981). Pozrikidis (1989) derived an alternative form in terms of derivatives of scalar functions and a Bessel transform with respect to the Cartesian coordinates parallel to the wall. This form is similar to that derived by Sommerfeld (1909) and Sommerfeld & Renner (1942) for electromagnetic radiation from a monochromatic dipole antenna opposite a dielectric and conducting half-space.

We show here that the Fourier transform with respect to time at fixed wavenumber can be inverted analytically. This allows evaluation of the flow field and the pressure at any point in space and time from a few one-dimensional numerical integrations

† Email address for correspondence: ufelder@physik.rwth-aachen.de

with respect to the wavenumber. Thus for the chosen initial condition one can follow in detail the evolution of the non-stationary viscous boundary layer in the framework of linear theory, starting from potential flow at short time (Schlichting 1987).

The Green function is relevant for the calculation of the velocity autocorrelation function of a Brownian particle located near a wall. The effect of the wall on the motion of the particle can be found approximately in terms of a reaction field tensor derived from the Green function at the position of the particle. In earlier work (Felderhof 2005*a*) we found the reaction field tensor for the no-slip boundary condition by first integrating over spatial wavenumber. This left a complicated frequency-dependent Fourier transform, requiring careful inversion to find the time dependence of the velocity autocorrelation function (Felderhof 2005*a*; Kraus 2007). The present formalism allows a much simpler calculation.

The theory is restricted to flow at low Reynolds number. For a discussion of the physical relevance we refer to the monographs by Happel & Brenner (1973) and by Kim & Karrila (1991).

## 2. Linear hydrodynamics in a half-space

We consider a viscous incompressible fluid of shear viscosity $\eta$ and mass density $\rho$ located in the half-space $z > 0$. For time $t < 0$ the fluid is at rest at constant pressure $p_0$. At time $t = 0$ an impulse $\boldsymbol{P}$ is imparted to the fluid at the point $\boldsymbol{r}_0 = (0, 0, h)$ at height $h$ on the $z$-axis. We study the resulting motion of the fluid for time $t > 0$.

For small-amplitude motion the flow velocity $\boldsymbol{v}(\boldsymbol{r}, t)$ and the pressure $p(\boldsymbol{r}, t)$ are governed by the linearized Navier–Stokes equations

$$\rho \frac{\partial \boldsymbol{v}}{\partial t} = \eta \nabla^2 \boldsymbol{v} - \nabla p + \boldsymbol{P}\delta(\boldsymbol{r} - \boldsymbol{r}_0)\delta(t), \qquad \nabla \cdot \boldsymbol{v} = 0. \tag{2.1}$$

The pressure $p(\boldsymbol{r}, t)$ is determined by the condition of incompressibility.

We consider first the case in which perfect slip boundary conditions apply at the plane $z = 0$. Then the flow velocity is easily found from the Green function $\boldsymbol{T}(\boldsymbol{r}, t)$ for the infinite fluid. It is given by

$$\boldsymbol{v}(\boldsymbol{r}, t) = \frac{1}{4\pi\eta}[\boldsymbol{T}(\boldsymbol{r} - \boldsymbol{r}_0, t) \cdot \boldsymbol{P} + \boldsymbol{T}(\boldsymbol{r} - \overline{\boldsymbol{r}}_0, t) \cdot \overline{\boldsymbol{P}}] \qquad \text{(slip)}, \tag{2.2}$$

where $\overline{\boldsymbol{r}}_0$ is the image point $\overline{\boldsymbol{r}}_0 = (0, 0, -h)$ and $\overline{\boldsymbol{P}} = (P_x, P_y, -P_z)$ is the image impulse. The explicit expression for the Green function $\boldsymbol{T}(\boldsymbol{r}, t)$ is known (Oseen 1927; Cichocki & Felderhof 2000):

$$\boldsymbol{T}(\boldsymbol{r}, t) = \mathbf{1}\frac{1}{\sqrt{4\pi\nu t}^{3/2}} \exp\left(-\frac{r^2}{4\nu t}\right) + \nu\nabla\nabla\frac{\operatorname{erf}(r/\sqrt{4\nu t})}{r}, \tag{2.3}$$

where $\nu = \eta/\rho$ is the kinematic viscosity. The tensor satisfies $\nabla \cdot \boldsymbol{T}(\boldsymbol{r}, t) = 0$. The pressure corresponding to (2.2) is

$$p(\boldsymbol{r}, t) = p_0 + \frac{1}{4\pi}\left[\frac{(\boldsymbol{r} - \boldsymbol{r}_0)}{|\boldsymbol{r} - \boldsymbol{r}_0|^3} \cdot \boldsymbol{P} + \frac{(\boldsymbol{r} - \overline{\boldsymbol{r}}_0)}{|\boldsymbol{r} - \overline{\boldsymbol{r}}_0|^3} \cdot \overline{\boldsymbol{P}}\right]\delta(t) \qquad \text{(slip)}. \tag{2.4}$$

The long-range pressure field is established instantaneously, because the fluid is incompressible. In the limit $t \to 0+$ one finds from (2.3)

$$\boldsymbol{T}(\boldsymbol{r}, 0+) = 4\pi\nu\mathbf{1}\delta(\boldsymbol{r}) + \nu\frac{-\mathbf{1} + 3\hat{\boldsymbol{r}}\hat{\boldsymbol{r}}}{r^3}, \tag{2.5}$$

so that at very short time the flow field $\boldsymbol{v}(\boldsymbol{r}, t)$ is a superposition of two dipolar potential flows.

For the no-slip boundary condition the flow velocity must vanish at the plane $z = 0$, and the solution is much more complicated. We write the flow velocity and the pressure in the form

$$\begin{aligned} \boldsymbol{v}(\boldsymbol{r}, t) &= \mathbf{G}(\boldsymbol{r}, \boldsymbol{r}_0, t) \cdot \boldsymbol{P}, \\ p(\boldsymbol{r}, t) &= p_0 + \boldsymbol{Q}(\boldsymbol{r}, \boldsymbol{r}_0, t) \cdot \boldsymbol{P} \qquad \text{(no-slip)}. \end{aligned} \tag{2.6}$$

In order to find $\boldsymbol{v}(\boldsymbol{r}, t)$ and $p(\boldsymbol{r}, t)$ we perform a Fourier transform with respect to the horizontal coordinates $(x, y)$ and also with respect to time. After Fourier analysis in time we find that the equations for the Fourier components

$$\boldsymbol{v}_\omega(\boldsymbol{r}) = \int_0^\infty \mathrm{e}^{\mathrm{i}\omega t} \boldsymbol{v}(\boldsymbol{r}, t)\, \mathrm{d}t, \qquad p_\omega(\boldsymbol{r}) = \int_0^\infty \mathrm{e}^{\mathrm{i}\omega t} [p(\boldsymbol{r}, t) - p_0]\, \mathrm{d}t \tag{2.7}$$

are

$$\eta(\nabla^2 \boldsymbol{v}_\omega - \alpha^2 \boldsymbol{v}_\omega) - \nabla p_\omega = -\boldsymbol{P}\delta(\boldsymbol{r} - \boldsymbol{r}_0), \qquad \nabla \cdot \boldsymbol{v}_\omega = 0, \tag{2.8}$$

where we have used the abbreviation

$$\alpha = (-\mathrm{i}\omega\rho/\eta)^{1/2}, \qquad \mathrm{Re}\alpha > 0. \tag{2.9}$$

The solution of (2.8) is expressed as

$$\boldsymbol{v}_\omega(\boldsymbol{r}) = \mathbf{G}_\omega(\boldsymbol{r}, \boldsymbol{r}_0) \cdot \boldsymbol{P}, \qquad p_\omega(\boldsymbol{r}) = \boldsymbol{Q}_\omega(\boldsymbol{r}, \boldsymbol{r}_0) \cdot \boldsymbol{P}. \tag{2.10}$$

Both Green functions $\mathbf{G}_\omega(\boldsymbol{r}, \boldsymbol{r}_0)$ and $\boldsymbol{Q}_\omega(\boldsymbol{r}, \boldsymbol{r}_0)$ can be expressed as Fourier integrals with respect to the $(x, y)$ coordinates:

$$\begin{aligned} \mathbf{G}_\omega(\boldsymbol{r}, \boldsymbol{r}_0) &= \int \exp[\mathrm{i}\boldsymbol{k} \cdot (\boldsymbol{s} - \boldsymbol{s}_0)]\ \hat{\mathbf{G}}(\boldsymbol{k}, \omega, z, h)\, \mathrm{d}\boldsymbol{k}, \\ \boldsymbol{Q}_\omega(\boldsymbol{r}, \boldsymbol{r}_0) &= \int \exp[\mathrm{i}\boldsymbol{k} \cdot (\boldsymbol{s} - \boldsymbol{s}_0)]\ \hat{\boldsymbol{Q}}(\boldsymbol{k}, \omega, z, h)\, \mathrm{d}\boldsymbol{k}, \end{aligned} \tag{2.11}$$

with two-dimensional vectors $\boldsymbol{s} = (x, y)$ and $\boldsymbol{k} = (k_x, k_y)$. The elements of the tensor $\mathbf{G}_\omega$ satisfy the reciprocity relation (Jones 1981)

$$G_{\omega,\alpha\beta}(\boldsymbol{r}, \boldsymbol{r}_0) = G_{\omega,\beta\alpha}(\boldsymbol{r}_0, \boldsymbol{r}). \tag{2.12}$$

Correspondingly the elements of the Fourier-transformed tensor are related by

$$\hat{G}_{\alpha\beta}(\boldsymbol{k}, \omega, z, h) = \hat{G}_{\beta\alpha}(-\boldsymbol{k}, \omega, h, z). \tag{2.13}$$

It turns out that the inverse transform with respect to the frequency of $\hat{\mathbf{G}}(\boldsymbol{k}, \omega, z, h)$ and $\hat{\boldsymbol{Q}}(\boldsymbol{k}, \omega, z, h)$ can be found in closed form. The calculation of the flow field $\boldsymbol{v}(\boldsymbol{r}, t)$ and the pressure $p(\boldsymbol{r}, t)$ can be reduced to a few single quadratures with respect to the wavenumber $k$. It will be convenient to consider separately the cases in which the impulse $\boldsymbol{P}$ is directed perpendicular and parallel to the wall. We note that corresponding results for a rotlet can be found by taking the curl of the solution.

## 3. Vertical excitation

In order to find the elements of the tensor $\hat{\mathbf{G}}(\boldsymbol{k}, \omega, z, h)$ one must solve a set of ordinary differential equations. We consider first the case in which the impulse $\boldsymbol{P}$ is in the $z$-direction, and consequently the flow is axially symmetric about the $z$-axis. For

this case it suffices to consider the elements $\hat{G}_{zz}(\boldsymbol{k},\omega,z,h)$ and $\hat{G}_{xz}(\boldsymbol{k},\omega,z,h)$. The expression for the element $\hat{G}_{zz}(\boldsymbol{k},\omega,z,h)$ is (Felderhof 2005*a*)

$$\hat{G}_{zz}(\boldsymbol{k},\omega,z,h)=\frac{k}{8\pi^2\eta s(k-s)\alpha^2}\big[s(k+s)\mathrm{e}^{-kh-kz}+s(k-s)\mathrm{e}^{-k|z-h|}-k(k-s)\times\mathrm{e}^{-s|z-h|}+k(k+s)\mathrm{e}^{-sh-sz}-2ks\mathrm{e}^{-kh-sz}-2ks\mathrm{e}^{-sh-kz}\big] \quad (3.1)$$

with the abbreviation

$$s=\sqrt{k^2+\alpha^2}. \quad (3.2)$$

The expression (3.1) agrees with that derived by Jones (1981) for a viscous compressible fluid, in the limit in which the fluid is incompressible. The expression for the element $\hat{G}_{xz}(\boldsymbol{k},\omega,z,h)$ is

$$\hat{G}_{xz}(\boldsymbol{k},\omega,z,h)=\frac{-\mathrm{i}k_x}{8\pi^2\eta(k-s)\alpha^2}\big[(k+s)\mathrm{e}^{-kh-kz}\pm(k-s)\mathrm{e}^{-k|z-h|}\mp(k-s)\times\mathrm{e}^{-s|z-h|}+(k+s)\mathrm{e}^{-sh-sz}-2s\mathrm{e}^{-kh-sz}-2k\mathrm{e}^{-sh-kz}\big], \quad (3.3)$$

with the upper sign for $z>h$ and the lower sign for $z<h$.

In order to perform the inverse Fourier transform of the above elements we use an identity derived elsewhere (Felderhof 2008),

$$\int_0^\infty \mathrm{e}^{\mathrm{i}\omega t}S_0(q,2k;x-2\nu kt,t)\,\mathrm{d}t=\frac{\mathrm{e}^{-\zeta x}}{\zeta-q}, \quad (3.4)$$

where the function $S_0(q,2k;x-2\nu kt,t)$ is given by

$$S_0(q,2k;u,t)=\sqrt{\frac{\nu}{\pi t}}\exp\left[-\frac{u^2}{4\nu t}\right]+\nu(q+k)\mathrm{e}^{-qu+\nu q^2t}\mathrm{erfc}\left(\frac{u}{\sqrt{4\nu t}}-q\sqrt{\nu t}\right), \quad (3.5)$$

and the variable $\zeta$ is defined by

$$\zeta=-k+\sqrt{k^2+\alpha^2}=-k+s. \quad (3.6)$$

The identity (3.4) holds, provided the integral on the left converges, i.e. provided the imaginary part of the complex variable $\omega$ is positive and sufficiently large. The identity follows from item 12 in Appendix V of Carslaw & Jaeger (1959) and use of theorem VI in § 12.2 in the same monograph. We note from (3.6) that $\alpha^2$ can be expressed as

$$\alpha^2=\zeta(\zeta+2k). \quad (3.7)$$

Taking the derivative in (3.4) with respect to $q$ and putting $q=0$ we find the related identity

$$\int_0^\infty \mathrm{e}^{\mathrm{i}\omega t}U(k;x-2\nu kt,t)\,\mathrm{d}t=\frac{\mathrm{e}^{-\zeta x}}{\zeta^2}, \quad (3.8)$$

with the function $U(k;u,t)$ given by

$$U(k;u,t)=\frac{2k\sqrt{\nu t}}{\sqrt{\pi}}\exp\left[-\frac{u^2}{4\nu t}\right]+(1-ku)\mathrm{erfc}\frac{u}{\sqrt{4\nu t}}. \quad (3.9)$$

We use cylindrical coordinates $(R,\varphi,z)$ and write

$$8\pi^2\rho\,\hat{G}_{zz}(\boldsymbol{k},z,h,t)=V_{zz}(k,z,h,t),\qquad 8\pi^2\rho\,\hat{G}_{xz}(\boldsymbol{k},z,h,t)=-\mathrm{i}V_{Rz}(k,z,h,t)\cos\varphi_{\boldsymbol{k}}, \quad (3.10)$$

where $\varphi_{\boldsymbol{k}}$ is the angle between the vector $\boldsymbol{k}$ and the $x$-axis. Decomposing the expression in (3.1) into partial fractions in the complex variable $\zeta$ we find for the inverse Fourier transform with respect to frequency

$$\begin{aligned} V_{zz}(k,z,h,t) = {} & 2k^2\sqrt{\frac{\tau}{\pi}}\mathrm{e}^{-k^2\tau}\left(\mathrm{e}^{-kh-z^2/4\tau}+\mathrm{e}^{-kz-h^2/4\tau}-\mathrm{e}^{-(h+z)^2/4\tau}-\mathrm{e}^{-k(h+z)}\right) \\ & -\frac{1}{2}k\Bigg[\mathrm{e}^{-k(h+z)}\Bigg((2+4k^2\tau)\operatorname{erf}(k\sqrt{\tau})+(1-2kh+4k^2\tau)\operatorname{erf}\frac{h-2k\tau}{2\sqrt{\tau}} \\ & +(1-2kz+4k^2\tau)\operatorname{erf}\frac{z-2k\tau}{2\sqrt{\tau}}+(2kh+2kz-4k^2\tau)\operatorname{erf}\frac{h+z-2k\tau}{2\sqrt{\tau}}\Bigg) \\ & +\mathrm{e}^{k(h-z)}\left(\operatorname{erf}\frac{h-z+2k\tau}{2\sqrt{\tau}}-\operatorname{erf}\frac{h+2k\tau}{2\sqrt{\tau}}\right) \\ & -\mathrm{e}^{-k(h-z)}\left(\operatorname{erf}\frac{h-z-2k\tau}{2\sqrt{\tau}}+\operatorname{erf}\frac{z+2k\tau}{2\sqrt{\tau}}\right)\Bigg], \end{aligned} \tag{3.11}$$

where we have abbreviated $\tau = \nu t$. Similarly we find for the second element

$$\begin{aligned} V_{Rz}(k,z,h,t) = {} & V_{zz}(k,z,h,t)+k\mathrm{e}^{-k(h+z)}\left(\operatorname{erf}\frac{h+z-2k\tau}{2\sqrt{\tau}}-\operatorname{erf}\frac{z-2k\tau}{2\sqrt{\tau}}\right) \\ & -k\mathrm{e}^{-k(h-z)}\left(\operatorname{erf}\frac{h-z-2k\tau}{2\sqrt{\tau}}+\operatorname{erf}\frac{z+2k\tau}{2\sqrt{\tau}}\right) = -\frac{1}{k}\frac{\partial V_{zz}(z,k,t)}{\partial z}. \end{aligned} \tag{3.12}$$

Both these expressions tend to zero as $t \to \infty$ for $h$, $z$ and $k$ positive. The axially symmetric flow generated by an impulse $\boldsymbol{P} = P\boldsymbol{e}_z$ in the $z$-direction has $z$-component

$$v_{zz}(\boldsymbol{r},t) = \frac{P}{4\pi\rho}\int_0^\infty V_{zz}(k,h,z,t)J_0(kR)k\,\mathrm{d}k \tag{3.13}$$

and $R$-component

$$v_{Rz}(\boldsymbol{r},t) = \frac{P}{4\pi\rho}\int_0^\infty V_{Rz}(k,h,z,t)J_1(kR)k\,\mathrm{d}k, \tag{3.14}$$

with Bessel functions $J_l(kR)$. The $\varphi$-component vanishes. The one-dimensional integrals are easily evaluated numerically. The second equality in (3.12) guarantees that the incompressibility condition $\nabla\cdot\boldsymbol{v}=0$ is satisfied. It can be checked that both components $v_{Rz}(\boldsymbol{r},t)$ and $v_{zz}(\boldsymbol{r},t)$ vanish at the plane $z=0$, so that the no-slip boundary condition is satisfied.

On account of the axial symmetry the flow may be derived from a Stokes streamfunction (Acheson 1990) according to

$$\boldsymbol{v}_z(\boldsymbol{r},t) = \nabla\times\left(\frac{\Psi(R,z,t)}{R}\,\boldsymbol{e}_\varphi\right). \tag{3.15}$$

The two non-vanishing components of the flow velocity are given by

$$v_{Rz}(\boldsymbol{r},t) = -\frac{1}{R}\frac{\partial\Psi(R,z,t)}{\partial z}, \qquad v_{zz}(\boldsymbol{r},t) = \frac{1}{R}\frac{\partial\Psi(R,z,t)}{\partial R}. \tag{3.16}$$

From (3.13) one finds

$$\Psi(\boldsymbol{r},t)=\frac{P}{4\pi\rho}R\int_0^\infty V_{zz}(k,h,z,t)J_1(kR)\,\mathrm{d}k. \tag{3.17}$$

The Stokes streamfunction is constant along the streamlines. This may be used to plot the streamlines.

The corresponding pressure is found from

$$p_z(\boldsymbol{r},t)=p_0+\frac{\nu P}{4\pi}\int_0^\infty \Pi_z(k,h,t)J_0(kR)\mathrm{e}^{-kz}k\,\mathrm{d}k, \tag{3.18}$$

where the function $\Pi_z(k,h,t)$ is calculated from the equation

$$\eta k\Pi_z\mathrm{e}^{-kz}=\rho\frac{\partial V_{zz}}{\partial t}+\eta\left(k^2V_{zz}-\frac{\partial^2V_{zz}}{\partial z^2}\right). \tag{3.19}$$

One finds

$$\Pi_z(k,h,t)=2k\left[\frac{\mathrm{e}^{-k^2\tau}}{\sqrt{\pi\tau}}\left(\mathrm{e}^{-h^2/4\tau}-\mathrm{e}^{-kh}\right)-k\ \mathrm{e}^{-kh}\ \mathrm{erf}(k\sqrt{\tau})-ke^{-kh}\ \mathrm{erf}\frac{h-2k\tau}{2\sqrt{\tau}}\right]. \tag{3.20}$$

At any time the pressure satisfies Laplace's equation $\nabla^2p_z=0$.

It is of interest to consider the behaviour of the amplitudes $V_{Rz}$, $V_{zz}$ and $\Pi_z$ at short time. The time scale of our problem is $\tau_h=h^2/\nu$. Keeping only the dominant terms as $\tau\to0$ one finds for $z>0$

$$\begin{aligned}
V_{Rz}^{sh}(k,z,h,t)&=\pm k\mathrm{e}^{-k|z-h|}-k\mathrm{e}^{-k(z+h)}-4k^2\mathrm{e}^{-k(z+h)}\sqrt{\frac{\tau}{\pi}}+O(\tau),\\
V_{zz}^{sh}(k,z,h,t)&=k\left[\mathrm{e}^{-k|z-h|}-\mathrm{e}^{-k(z+h)}\right]-4k^2\mathrm{e}^{-k(z+h)}\sqrt{\frac{\tau}{\pi}}+O(\tau),\\
\Pi_z^{sh}(k,h,t)&=-2k\mathrm{e}^{-kh}\left[\frac{1}{\sqrt{\pi\tau}}+k\right]+O(\sqrt{\tau}),
\end{aligned} \tag{3.21}$$

with sign convention as in (3.3). The corresponding short-time expressions for flow and pressure can be derived from the dipole potentials

$$\phi(\boldsymbol{r})=\Phi(\boldsymbol{r}-\boldsymbol{r}_0),\qquad \overline{\phi}(\boldsymbol{r})=\Phi(\boldsymbol{r}-\overline{\boldsymbol{r}}_0), \tag{3.22}$$

with the abbreviation

$$\Phi(\boldsymbol{r})=\frac{1}{4\pi\rho}\frac{zP}{r^3}. \tag{3.23}$$

In cylindrical coordinates

$$\phi(\boldsymbol{r})=\frac{z-h}{\left[R^2+(z-h)^2\right]^{3/2}}\frac{P}{4\pi\rho},\qquad \overline{\phi}(\boldsymbol{r})=\frac{z+h}{[R^2+(z+h)^2]^{3/2}}\frac{P}{4\pi\rho}. \tag{3.24}$$

In terms of these potentials the short-time flow velocity is

$$\begin{aligned}
v_{Rz}^{sh}(\boldsymbol{r},t)&=-\frac{\partial\phi}{\partial R}+\frac{\partial\overline{\phi}}{\partial R}-4\sqrt{\frac{\tau}{\pi}}\frac{\partial^2\overline{\phi}}{\partial R\partial z}+O(\tau),\\
v_{zz}^{sh}(\boldsymbol{r},t)&=-\frac{\partial\phi}{\partial z}+\frac{\partial\overline{\phi}}{\partial z}-4\sqrt{\frac{\tau}{\pi}}\frac{\partial^2\overline{\phi}}{\partial z^2}+O(\tau),
\end{aligned} \tag{3.25}$$

and the short-time pressure is

$$p_z^{sh}(\boldsymbol{r}, t) = p_0 + \frac{2\eta}{\sqrt{\pi\tau}}\frac{\partial\overline{\phi}}{\partial z} - 2\eta\frac{\partial^2\overline{\phi}}{\partial z^2} + O(\sqrt{\tau}). \tag{3.26}$$

Alternatively we may write in vector form

$$\boldsymbol{v}_z^{sh}(\boldsymbol{r}, t) = -\nabla\phi + \nabla\overline{\phi} - 4\sqrt{\frac{\tau}{\pi}}\nabla\frac{\partial\overline{\phi}}{\partial h} + O(\tau). \tag{3.27}$$

Therefore, up to terms of order $\tau$, the short-time flow is irrotational. The short-time flow velocity and the short-time pressure are related by

$$\rho\frac{\partial\boldsymbol{v}_z^{sh}}{\partial t} = -\nabla p_z^{sh} + O(1). \tag{3.28}$$

We note that (3.27) and (3.28) must be regarded as asymptotic expansions in $\tau$ valid for fixed $z > 0$. The short-time correction to the pressure is clearly due to viscous effects. It may also be written as

$$\delta p_z^{sh}(\boldsymbol{r}, t) = \frac{2\eta}{\sqrt{\pi\tau}}\frac{\partial\overline{\phi}}{\partial h} - 2\eta\frac{\partial^2\overline{\phi}}{\partial h^2} + O(\sqrt{\tau}). \tag{3.29}$$

The short-time pressure disturbance diverges in the limit $t \to 0$, and it follows from (3.24) that it extends over large distances. In cylindrical coordinates

$$\frac{\partial\overline{\phi}}{\partial h} = \frac{R^2 - 2(z+h)^2}{\left[R^2 + (z+h)^2\right]^{5/2}}\frac{P}{4\pi\rho}. \tag{3.30}$$

For $P < 0$, i.e. for an impulse directed towards the plane, there is an increase of pressure in the plane $z = z_0$ within a circle of radius $R_0 = \sqrt{2}(z_0 + h)$. Outside the circle there is a decrease of pressure, falling off as $R^{-3}$ at large distance from the $z$-axis. The integral over the plane vanishes.

The flow pattern and pressure at any time $t$ may be evaluated by numerical integration in (3.13), (3.14) and (3.18). We choose units such that $\eta = 1$, $\rho = 1$, $h = 1$. The impulse generates an axially symmetric vortex ring. In figure 1 we show the streamlines in the $Rz$-plane at time $t = 0.5$. At this time the centre of the vortex ring, where $v_{Rz}$ and $v_{zz}$ vanish, is at $(R, z) = (1.77, 1.83)$. At short times the flow pattern is well approximated by (2.2) for perfect slip boundary conditions, except close to the wall, where it is strongly suppressed. At later times the flow is still qualitatively the same as that for slip boundary conditions, except close to the wall, though reduced in magnitude. As an example we show in figure 2 the $z$-component of the flow velocity in the $xz$-plane at $z = 0.5$ and $t = 0.5$ as a function of $x$ and compare with that for the slip boundary condition. In figure 3 we present results for the $x$-component of the flow velocity and make the same comparison. At any fixed time the flow far from the wall is nearly identical with that for the slip boundary condition.

The main qualitative difference with the flow for the perfect slip boundary condition is that for the no-slip condition there is a pressure disturbance at all times. At short times the pressure disturbance is large. In figure 4 we plot the pressure disturbance in the $xz$-plane at time $t = 0.5$. The pressure disturbance decays monotonically in time.

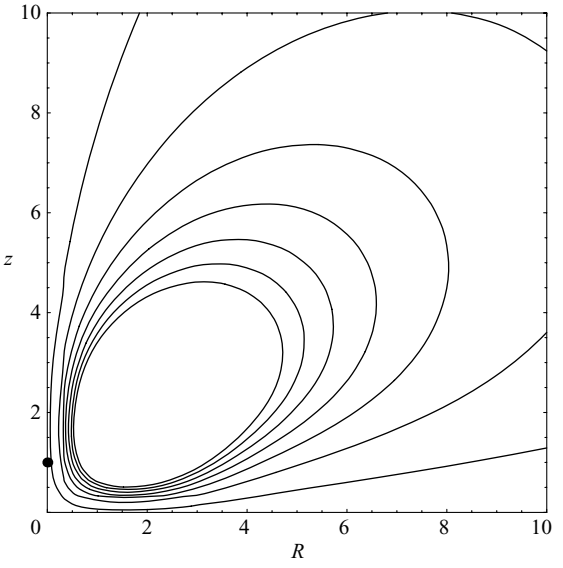


FIGURE 1. Streamlines in the $Rz$-plane at time $t = 0.5$ after a sudden impulse in the $z$-direction at time $t = 0$ at the point $\boldsymbol{r}_0 = (0, 0, 1)$ for the no-slip boundary condition at the plane $z = 0$.

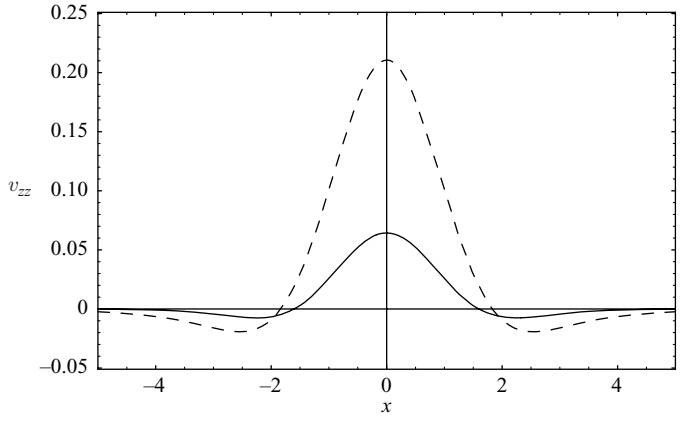


FIGURE 2. The $z$-component of the flow velocity in the $xz$-plane at height $z = 0.5$ at time $t = 0.5$ after a sudden impulse of strength $P = 4\pi$ in the positive $z$-direction at time $t = 0$ at the point $\boldsymbol{r}_0 = (0, 0, 1)$ for the no-slip boundary condition at the plane $z = 0$ (solid curve), compared with that for the perfect slip boundary condition (dashed curve).

## 4. Horizontal excitation

Next we consider the case in which the impulse $\boldsymbol{P}$ is in the $x$-direction. In this case the axial symmetry about the $z$-axis is lost. In order to find the flow pattern we must consider the three elements $\hat{G}_{xx}(\boldsymbol{k}, \omega, z, h)$, $\hat{G}_{yx}(\boldsymbol{k}, \omega, z, h)$ and $\hat{G}_{zx}(\boldsymbol{k}, \omega, z, h)$.

The expression for the element $\hat{G}_{xx}(\boldsymbol{k}, \omega, z, h)$ is (Felderhof 2005*a*)

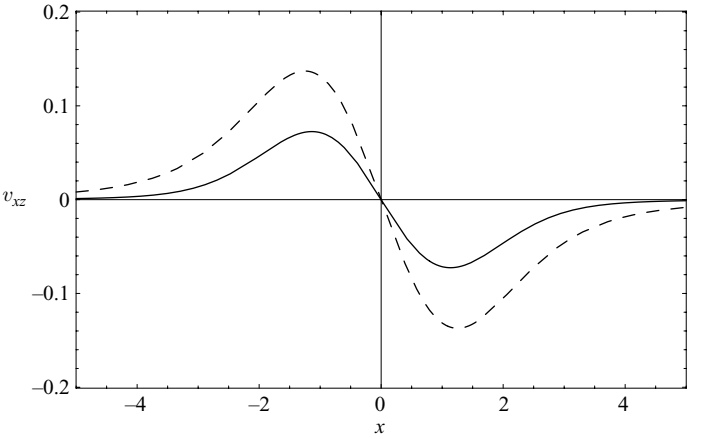


FIGURE 3. The $x$-component of the flow velocity in the $xz$-plane at height $z=0.5$ at time $t=0.5$ after a sudden impulse of strength $P=4\pi$ in the positive $z$-direction at time $t=0$ at the point $\boldsymbol{r}_0=(0,0,1)$ for no-slip boundary condition at the plane $z=0$ (solid curve), compared with that for the perfect slip boundary condition (dashed curve).

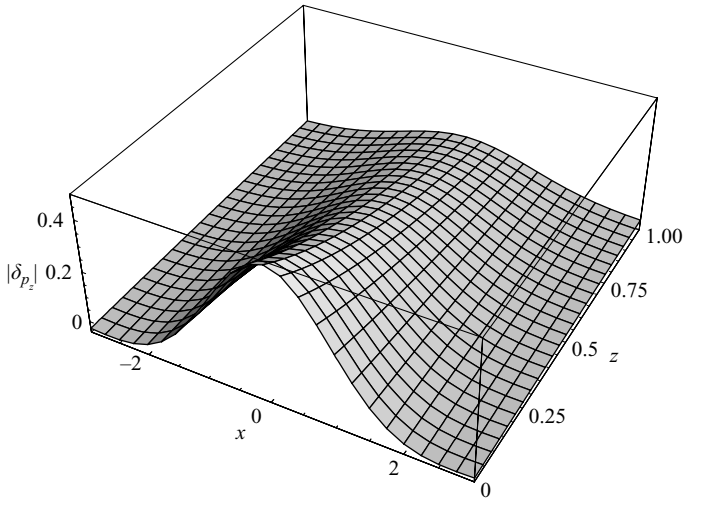


FIGURE 4. Plot of the pressure disturbance $|\delta p_z|$ in the $xz$-plane at time $t=0.5$ after a sudden impulse of strength $P=4\pi$ in the $z$-direction at time $t=0$ at the point $\boldsymbol{r}_0=(0,0,1)$ for the no-slip boundary condition at the plane $z=0$.

$$\begin{aligned}\hat{G}_{xx}(\boldsymbol{k},\omega,z,h)=\frac{1}{8\pi^2\eta k\alpha^2}\Bigg[&\frac{k}{k-s}(k(k+s)\mathrm{e}^{-kh-kz}-k(k-s)\mathrm{e}^{-k|z-h|}+s(k-s)\mathrm{e}^{-s|z-h|}\\&+s(k+s)\mathrm{e}^{-sh-sz}-2ks\mathrm{e}^{-kh-sz}-2ks\mathrm{e}^{-sh-kz})\\&+\frac{k_y^2(k+s)}{\alpha^2 s}(s(k+s)\mathrm{e}^{-kh-kz}-s(k-s)\mathrm{e}^{-k|z-h|}+k(k-s)\mathrm{e}^{-s|z-h|}\\&-(k^2-ks-2s^2)\mathrm{e}^{-sh-sz}-2s^2\mathrm{e}^{-kh-sz}-2s^2\mathrm{e}^{-sh-kz})\Bigg]\end{aligned}\tag{4.1}$$

with $k_y^2 = k^2 - k_x^2$. We write

$$8\pi^2\rho\hat{G}_{xx}(\boldsymbol{k}, z, h, t) = V_{xx0}(k, z, h, t) + V_{xxc}(k, z, h, t)\cos^2\varphi_{\boldsymbol{k}}, \tag{4.2}$$

where $V_{xxc}(k, z, h, t)\cos^2\varphi_{\boldsymbol{k}}$ originates from the terms in proportion to $k_x^2$, and $V_{xx0}(k, z, h, t)$ originates from the remaining terms. We find

$$V_{xx0}(k, z, h, t) = \frac{1}{\sqrt{\pi\tau}}\mathrm{e}^{-k^2\tau}\left(\mathrm{e}^{-(z-h)^2/4\tau} - \mathrm{e}^{-(z+h)^2/4\tau}\right) \tag{4.3}$$

and

$$\begin{aligned} V_{xxc}(k, z, h, t) = V_{zz}(k, z, h, t) &+ k\mathrm{e}^{-k(h+z)}\left(2\mathrm{erf}\frac{h+z-2k\tau}{2\sqrt{\tau}} - \mathrm{erf}\frac{z-2k\tau}{2\sqrt{\tau}} - \mathrm{erf}\frac{h-2k\tau}{2\sqrt{\tau}}\right) \\ &- k\mathrm{e}^{-k(h-z)}\left(\mathrm{erf}\frac{h-z-2k\tau}{2\sqrt{\tau}} + \mathrm{erf}\frac{z+2k\tau}{2\sqrt{\tau}}\right) \\ &+ k\mathrm{e}^{k(h-z)}\left(\mathrm{erf}\frac{h-z+2k\tau}{2\sqrt{\tau}} - \mathrm{erf}\frac{h+2k\tau}{2\sqrt{\tau}}\right). \end{aligned} \tag{4.4}$$

Both these expressions tend to zero as $t \to \infty$ for $h$, $z$ and $k$ positive. The flow generated by an impulse $\boldsymbol{P} = P\boldsymbol{e}_x$ in the $x$-direction has $x$-component

$$\begin{aligned} v_{xx}(\boldsymbol{r}, t) = v_{xx0}(\boldsymbol{r}, t) + \frac{P}{4\pi\rho}\Bigg[&\int_0^\infty V_{xxc}(k, h, z, t)J_1(kR)/R\ \mathrm{d}k \\ &- \cos^2\varphi\int_0^\infty V_{xxc}(k, h, z, t)J_2(kR)k\ \mathrm{d}k\Bigg] \end{aligned} \tag{4.5}$$

with the first term given by

$$\begin{aligned} v_{xx0}(\boldsymbol{r}, t) &= \frac{P}{4\pi\rho}\int_0^\infty V_{xx0}(k, h, z, t)J_0(kR)k\ \mathrm{d}k \\ &= \frac{P}{4\pi\rho}\frac{\mathrm{e}^{-R^2/4\tau}}{\sqrt{4\pi}\tau^{3/2}}\left(\mathrm{e}^{-(z-h)^2/4\tau} - \mathrm{e}^{-(z+h)^2/4\tau}\right). \end{aligned} \tag{4.6}$$

The expression for the element $\hat{G}_{yx}(\boldsymbol{k}, \omega, z, h)$ is

$$\begin{aligned} \hat{G}_{yx}(\boldsymbol{k}, \omega, z, h) = \frac{k_x k_y}{8\pi^2\eta k(k-s)\alpha^2}&[s(k+s)\mathrm{e}^{-kh-kz} - s(k-s)\mathrm{e}^{-k|z-h|} + k(k-s)\mathrm{e}^{-s|z-h|} \\ &- (k^2 - ks - 2s^2)\mathrm{e}^{-sh-sz} - 2s^2\mathrm{e}^{-kh-sz} - 2s^2\mathrm{e}^{-sh-kz}]. \end{aligned} \tag{4.7}$$

We write

$$8\pi^2\rho\hat{G}_{yx}(\boldsymbol{k}, z, h, t) = V_{yx}(k, z, h, t)\sin\varphi_{\boldsymbol{k}}\cos\varphi_{\boldsymbol{k}} \tag{4.8}$$

and find

$$V_{yx}(k, z, h, t) = V_{xxc}(k, z, h, t). \tag{4.9}$$

The flow generated by an impulse $\boldsymbol{P} = P\boldsymbol{e}_x$ in the $x$-direction has $y$-component

$$v_{yx}(\boldsymbol{r}, t) = -\frac{P}{4\pi\rho}\sin\varphi\cos\varphi\int_0^\infty V_{xxc}(k, h, z, t)J_2(kR)k\ \mathrm{d}k. \tag{4.10}$$

The element $\hat{G}_{zx}(\boldsymbol{k}, \omega, z, h)$ may be found from (3.3) by use of the reciprocity relation (2.13). This yields

$$\hat{G}_{zx}(\boldsymbol{k}, \omega, z, h) = -\hat{G}_{xz}(\boldsymbol{k}, \omega, h, z). \tag{4.11}$$

We write

$$8\pi^2\rho\hat{G}_{zx}(\boldsymbol{k},z,h,t)=\mathrm{i}V_{zx}(k,z,h,t)\cos\varphi_{\boldsymbol{k}} \tag{4.12}$$

and find

$$V_{zx}(k,z,h,t)=V_{zz}(k,z,h,t)+k\mathrm{e}^{-k(h+z)}\left(\mathrm{erf}\frac{h+z-2k\tau}{2\sqrt{\tau}}-\mathrm{erf}\frac{h-2k\tau}{2\sqrt{\tau}}\right)$$
$$+k\mathrm{e}^{k(h-z)}\left(\mathrm{erf}\frac{h-z+2k\tau}{2\sqrt{\tau}}-\mathrm{erf}\frac{h+2k\tau}{2\sqrt{\tau}}\right). \tag{4.13}$$

The flow has $z$-component

$$v_{zx}(\boldsymbol{r},t)=-\frac{P}{4\pi\rho}\cos\varphi\int_0^\infty V_{zx}(k,h,z,t)J_1(kR)k\,\mathrm{d}k. \tag{4.14}$$

It can be checked that the three components $v_{xx}(\boldsymbol{r},t)$, $v_{yx}(\boldsymbol{r},t)$ and $v_{zx}(\boldsymbol{r},t)$ vanish at the plane $z=0$, so that the no-slip boundary condition is satisfied. The three elements are related by

$$\mathrm{i}k_x\hat{G}_{xx}(\boldsymbol{k},z,h,t)+\mathrm{i}k_y\hat{G}_{yx}(\boldsymbol{k},z,h,t)+\frac{\partial}{\partial z}\hat{G}_{zx}(\boldsymbol{k},z,h,t)=0, \tag{4.15}$$

so that the condition of incompressibility is satisfied.

The pressure corresponding to the above flow velocity is found from

$$p_x(\boldsymbol{r},t)=p_0-\frac{\nu P}{4\pi}\cos\varphi\int_0^\infty \Pi_x(k,h,t)J_1(kR)\mathrm{e}^{-kz}k\,\mathrm{d}k, \tag{4.16}$$

where the function $\Pi_x(k,h,t)$ is calculated from the equation

$$\eta k\Pi_x\mathrm{e}^{-kz}=\rho\frac{\partial V_{zx}}{\partial t}+\eta\left(k^2V_{zx}-\frac{\partial^2V_{zx}}{\partial z^2}\right). \tag{4.17}$$

One finds

$$\Pi_x(k,h,t)=\Pi_z(k,h,t)+\frac{h}{\sqrt{\pi}\tau^{3/2}}\mathrm{e}^{-k^2\tau-h^2/4\tau}. \tag{4.18}$$

At any time the pressure satisfies Laplace's equation, $\nabla^2p_x=0$. It follows from (4.16) that in the $yz$-plane the pressure disturbance $\delta p_x=p_x-p_0$ vanishes at any time.

It is of interest to consider the behaviour of the amplitudes $V_{xx0}$, $V_{yx}$, $V_{zx}$ and $\Pi_x$ for short time. Keeping only the dominant terms as $\tau\to0$ one finds for $z>0$

$$V^{sh}_{xx0}(k,z,h,t)=0,\quad V^{sh}_{xxc}(k,z,h,t)=-k\mathrm{e}^{-k|z-h|}-k\mathrm{e}^{-k(z+h)}-4k^2\mathrm{e}^{-k(h+z)}\sqrt{\frac{\tau}{\pi}}+O(\tau),$$

$$V^{sh}_{yx}(k,z,h,t)=-k\mathrm{e}^{-k|z-h|}-k\mathrm{e}^{-k(z+h)}-4k^2\mathrm{e}^{-k(h+z)}\sqrt{\frac{\tau}{\pi}}+O(\tau),$$

$$V^{sh}_{zx}(k,z,h,t)=\mp k\mathrm{e}^{-k|z-h|}-k\mathrm{e}^{-k(z+h)}-4k^2\mathrm{e}^{-k(h+z)}\sqrt{\frac{\tau}{\pi}}+O(\tau),$$

$$\Pi^{sh}_x(k,h,t)=-2k\mathrm{e}^{-kh}\left[\frac{1}{\sqrt{\pi\tau}}+k\right]+O(\sqrt{\tau}). \tag{4.19}$$

The corresponding expressions for short-time flow and pressure can be derived from the dipole potentials

$$\phi(\boldsymbol{r})=\Phi(\boldsymbol{r}-\boldsymbol{r}_0),\qquad \overline{\phi}(\boldsymbol{r})=\Phi(\boldsymbol{r}-\overline{\boldsymbol{r}}_0), \tag{4.20}$$

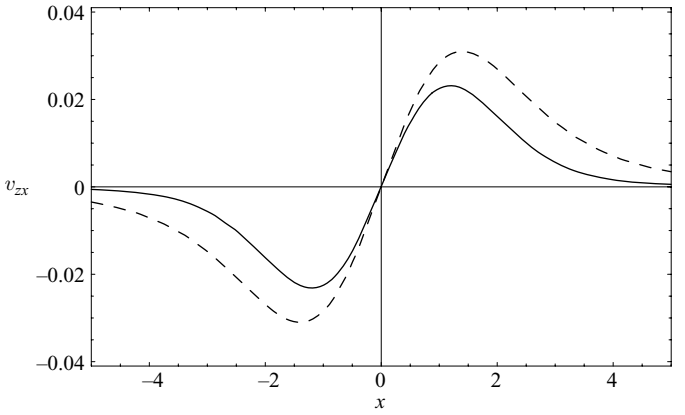


FIGURE 5. The $z$-component of the flow velocity in the $xz$-plane at height $z = 0.5$ at time $t = 0.5$ after a sudden impulse of strength $P = 4\pi$ in the positive $x$-direction at time $t = 0$ at the point $\boldsymbol{r}_0 = (0, 0, 1)$ for the no-slip boundary condition at the plane $z = 0$ (solid curve), compared with that for the perfect slip boundary condition (dashed curve).

with the abbreviation

$$\Phi(\boldsymbol{r}) = \frac{1}{4\pi\rho}\frac{xP}{r^3}. \tag{4.21}$$

In terms of these potentials the short-time flow velocity is

$$\boldsymbol{v}_x^{sh}(\boldsymbol{r}, t) = -\nabla\phi - \nabla\overline{\phi} + 4\sqrt{\frac{\tau}{\pi}}\nabla\frac{\partial\overline{\phi}}{\partial h} + O(\tau), \tag{4.22}$$

and the short-time pressure is

$$p_x^{sh}(\boldsymbol{r}, t) = p_0 - \frac{2\eta}{\sqrt{\pi\tau}}\frac{\partial\overline{\phi}}{\partial h} + 2\eta\frac{\partial^2\overline{\phi}}{\partial h^2} + O(\sqrt{\tau}). \tag{4.23}$$

Therefore, up to the terms of order $\tau$, the short-time flow is irrotational. The short-time flow velocity and the short-time pressure are related as in (3.28). In Cartesian coordinates

$$\frac{\partial\overline{\phi}}{\partial h} = \frac{-3x(z+h)}{[x^2 + y^2 + (z+h)^2]^{5/2}}\frac{P}{4\pi\rho}. \tag{4.24}$$

For $P > 0$ there is at short times a pressure increase for $x > 0$ and a decrease for $x < 0$.

The flow pattern and pressure at any time $t$ may be evaluated by numerical integration in (4.5), (4.10) and (4.14). At short times the flow pattern is well approximated by (2.2) for perfect slip boundary conditions, except close to the wall, where it is strongly suppressed. At later times the flow is still qualitatively the same as that for slip boundary conditions, except close to the wall, though reduced in magnitude. As an example we show in figure 5 the $z$-component of the flow velocity in the $xz$-plane at $z = 0.5$ and $t = 0.5$ as a function of $x$ and compare with that for the slip boundary condition. In figure 6 we present results for the $x$-component of the flow velocity and make the same comparison. At any fixed time the flow far from the wall is nearly identical with that for the slip boundary condition.

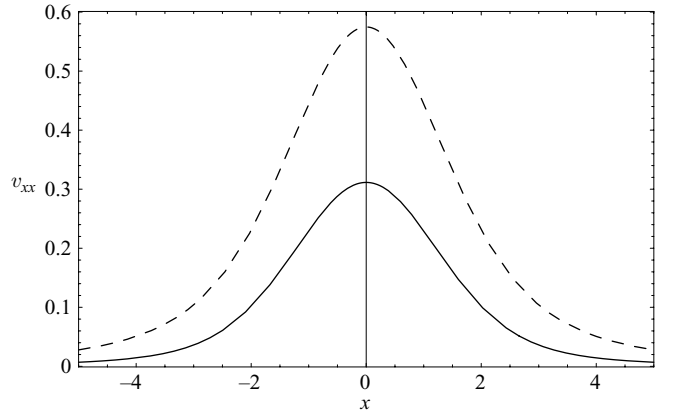


FIGURE 6. The $x$-component of the flow velocity in the $xz$-plane at height $z = 0.5$ at time $t = 0.5$ after a sudden impulse of strength $P = 4\pi$ in the positive $x$-direction at time $t = 0$ at the point $\boldsymbol{r}_0 = (0, 0, 1)$ for no-slip boundary condition at the plane $z = 0$ (solid curve), compared with that for the perfect slip boundary condition (dashed curve).

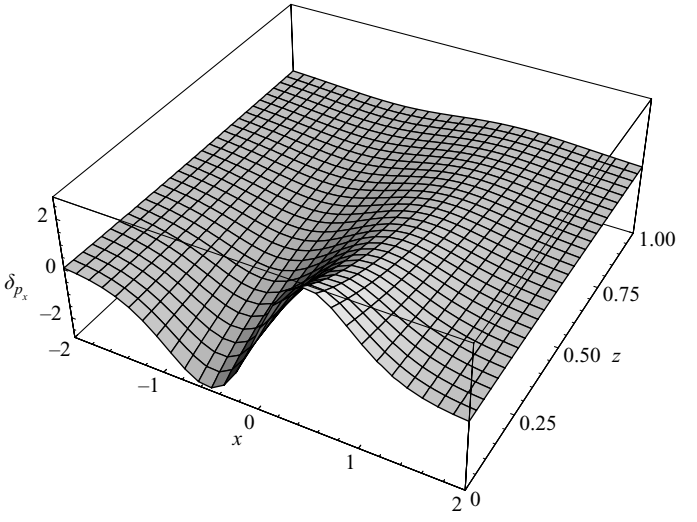


FIGURE 7. Plot of the pressure disturbance $\delta p_x$ in the $xz$-plane at time $t = 0.1$ after a sudden impulse of strength $P = 4\pi$ in the positive $x$-direction at time $t = 0$ at the point $\boldsymbol{r}_0 = (0, 0, 1)$ for the no-slip boundary condition at the plane $z = 0$.

There is a pressure disturbance which shows an oscillation in time. At short times the pressure disturbance is large. In figure 7 we plot the pressure disturbance in the $xz$-plane at time $t = 0.1$. We show in figure 8 how it has evolved at time $t = 0.5$.

## 5. Reaction field tensor

In earlier work (Felderhof 2005*a*) we have evaluated the velocity autocorrelation function of a Brownian particle of mass $m_p$ near a wall with the no-slip boundary condition in the limit in which the radius $a$ of the particle is small compared to the distance $h$ from the wall. The velocity autocorrelation function may be evaluated as the Fourier transform of the frequency-dependent admittance tensor. The latter

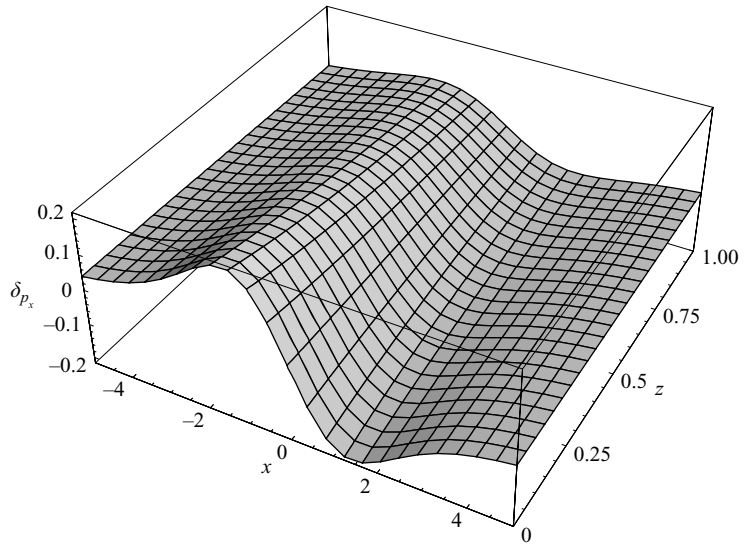


FIGURE 8. Plot of the pressure disturbance $\delta p_x$ in the $xz$-plane at time $t = 0.5$ after a sudden impulse of strength $P = 4\pi$ in the positive $x$-direction at time $t = 0$ at the point $\boldsymbol{r}_0 = (0, 0, 1)$ for no-slip boundary condition at the plane $z = 0$.

gives the mean velocity response of the particle to an applied harmonic force. The admittance tensor differs from that for infinite space due to the no-slip boundary condition applied at the wall. For $a \ll h$ the difference may be expressed in terms of a reaction field tensor $\boldsymbol{F}(\boldsymbol{r}_0, \omega)$ defined by

$$\boldsymbol{F}(\boldsymbol{r}_0, \omega) = \lim_{\boldsymbol{r} \to \boldsymbol{r}_0} (\boldsymbol{G}_\omega(\boldsymbol{r}, \boldsymbol{r}_0) - \boldsymbol{G}_{0\omega}(\boldsymbol{r} - \boldsymbol{r}_0)), \tag{5.1}$$

where $\boldsymbol{G}_{0\omega}(\boldsymbol{r} - \boldsymbol{r}_0)$ is the Green function tensor for infinite space. The tensor takes account of the backflow at the position of the particle. It follows from the reciprocity relation (2.12) that the tensor is symmetric. In the earlier work the two Green functions were expressed by spatial Fourier integrals as in (2.11). The subsequent integral over wave vector $\boldsymbol{k}$ could be evaluated in closed form as a function of frequency. The dependence on frequency is quite complicated, and the numerical calculation of the inverse Fourier transform, needed to obtain the reaction field as a function of time, requires care (Felderhof 2005*a*; Kraus 2007). The present formalism provides a simpler calculation of the reaction field.

The admittance tensor for a particle centred at $\boldsymbol{r}_0$ is

$$\mathscr{Y}(\boldsymbol{r}_0, \omega) = \mathscr{Y}_0(\omega)\left[\boldsymbol{1} + 6\pi\eta a\left(1 + \alpha a + \frac{1}{3}\alpha^2 a^2\right)\boldsymbol{F}(\boldsymbol{r}_0, \omega)\right], \tag{5.2}$$

where $\mathscr{Y}_0(\omega)$ is the scalar admittance for infinite space:

$$\mathscr{Y}_0(\omega) = \left[-\mathrm{i}\omega m_p + 6\pi\eta a\left(1 + \alpha a + \frac{1}{9}\alpha^2 a^2\right)\right]^{-1}. \tag{5.3}$$

In the theory of Brownian motion the velocity autocorrelation function of the particle is defined by

$$\boldsymbol{C}(t) = \langle \boldsymbol{U}(t)\boldsymbol{U}(0)\rangle, \tag{5.4}$$

where the angle brackets denote the equilibrium ensemble average. According to the fluctuation-dissipation theorem its Fourier transform is given by

$$\hat{\mathbf{C}}(\omega) = \int_0^\infty \mathrm{e}^{\mathrm{i}\omega t}\mathbf{C}(t)\,\mathrm{d}t = k_B T \mathscr{Y}(\boldsymbol{r}_0, \omega). \tag{5.5}$$

We consider first the case of vertical excitation. The analogue of (3.11) for the infinite space Green function is given by

$$V_{0zz}(k, z, h, t) = \frac{1}{2}k\left[\mathrm{e}^{k(h-z)}\left(1 - \mathrm{erf}\frac{h - z + 2k\tau}{2\sqrt{\tau}}\right) + \mathrm{e}^{-k(h-z)}\left(1 + \mathrm{erf}\frac{h - z - 2k\tau}{2\sqrt{\tau}}\right)\right]. \tag{5.6}$$

The difference function at $z = h$

$$\delta V_{zz}(k, h, t) = V_{zz}(k, h, h, t) - V_{0zz}(k, h, h, t) \tag{5.7}$$

is given by

$$\begin{aligned}\delta V_{zz}(k, h, t) = -k\Bigg[1 + 2k\sqrt{\frac{\tau}{\pi}}\left(\mathrm{e}^{-2kh-k^2\tau} - 2\mathrm{e}^{-(h+2k\tau)^2/4\tau} + \mathrm{e}^{-k^2\tau-h^2/\tau}\right)\\ + (1 + 2k^2\tau)\mathrm{e}^{-2kh}\mathrm{erf}\,k\sqrt{\tau} + (1 - 2kh + 4k^2\tau)\mathrm{e}^{-2kh}\mathrm{erf}\frac{h - 2k\tau}{2\sqrt{\tau}}\\ + 2(kh - k^2\tau)\mathrm{e}^{-2kh}\mathrm{erf}\frac{h - k\tau}{\sqrt{\tau}} - \mathrm{erf}\frac{h + k\tau}{\sqrt{\tau}}\Bigg].\end{aligned} \tag{5.8}$$

The corresponding relaxation function, characterizing the time-dependent reaction field, is defined by

$$\psi_z(\tau) = \frac{3}{2}\int_0^\infty \delta V_{zz}(k, h, t)k\,\mathrm{d}k. \tag{5.9}$$

The reaction field factor is given by

$$F_{zz}(\boldsymbol{r}_0, \omega) = \frac{1}{6\pi\rho}\int_0^\infty \mathrm{e}^{\mathrm{i}\omega t}\psi_z(\tau)\,\mathrm{d}t. \tag{5.10}$$

At time $t = 0$

$$\delta V_{zz}(k, h, 0) = -k\mathrm{e}^{-2kh}. \tag{5.11}$$

Hence the initial value of the relaxation function is

$$\psi_z(0) = -\frac{3}{8h^3}, \tag{5.12}$$

in agreement with the earlier result found from the high-frequency behaviour of the Fourier transform. From the low-frequency behaviour of the Fourier transform we found that at long times the relaxation function decays as

$$\psi_z(\tau) \approx -\frac{1}{2\sqrt{\pi}}\tau^{-3/2} \qquad \text{as } \tau \to \infty, \tag{5.13}$$

independent of the distance from the wall. The behaviour at intermediate times is found easily from (5.9) by numerical integration. In figure 9 we plot $\log[\psi_z(\tau)/\psi_z(0)]$ as a function of $\log_{10}(\tau/h^2)$.

Next we consider the case of horizontal excitation. The analogue of (4.4) for the infinite space Green function is given by

$$V_{0xxc}(k, z, h, t) = -V_{0zz}(k, z, h, t). \tag{5.14}$$

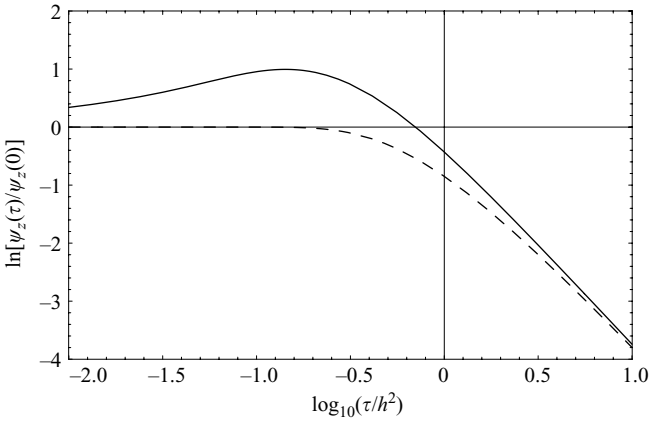


FIGURE 9. Plot of $\ln[\psi_z(\tau)/\psi_z(0)]$ for the no-slip boundary condition (solid curve) and for perfect slip boundary condition (dashed curve) as functions of $\log_{10}(\tau/h^2)$.

We define the difference function

$$\delta V_{xx}(k,h,t) = V_{xxc}(k,h,h,t) - V_{0xxc}(k,h,h,t). \tag{5.15}$$

It is given by

$$\delta V_{xx}(k,h,t) = \delta V_{zz}(k,h,t) + 2k\,\mathrm{erfc}\frac{h+2k\tau}{2\sqrt{\tau}} + 2k\mathrm{e}^{-2kh}\left(\mathrm{erf}\frac{h-k\tau}{\sqrt{\tau}} - \mathrm{erf}\frac{h-2k\tau}{2\sqrt{\tau}}\right). \tag{5.16}$$

The corresponding relaxation function, characterizing the time-dependent reaction field, is defined by

$$\psi_x(\tau) = -\frac{3}{4\sqrt{\pi}\tau^{3/2}}\,\mathrm{e}^{-h^2/4\tau} + \frac{3}{4}\int_0^\infty \delta V_{xx}(k,h,t)k\,\mathrm{d}k. \tag{5.17}$$

The first term arises from the function $V_{xx0}$ in (4.3) and from the corresponding

$$V_{0xx0}(k,h,t) = \frac{1}{\sqrt{\pi\tau}}\,\mathrm{e}^{-k^2\tau-(z-h)^2/4\tau}. \tag{5.18}$$

The reaction field factor is given by

$$F_{xx}(\boldsymbol{r}_0,\omega) = \frac{1}{6\pi\rho}\int_0^\infty \mathrm{e}^{\mathrm{i}\omega t}\psi_x(\tau)\,\mathrm{d}t. \tag{5.19}$$

At time $t=0$

$$\delta V_{xx}(k,h,0) = \delta V_{zz}(k,h,0). \tag{5.20}$$

Hence the initial value of the relaxation function is

$$\psi_x(0) = -\frac{3}{16h^3}, \tag{5.21}$$

in agreement with the earlier result found from the Fourier transform. From the low-frequency behaviour of the Fourier transform we found that at long times the relaxation function decays as

$$\psi_x(\tau) \approx -\frac{1}{2\sqrt{\pi}}\tau^{-3/2} \qquad \text{as } \tau\to\infty. \tag{5.22}$$

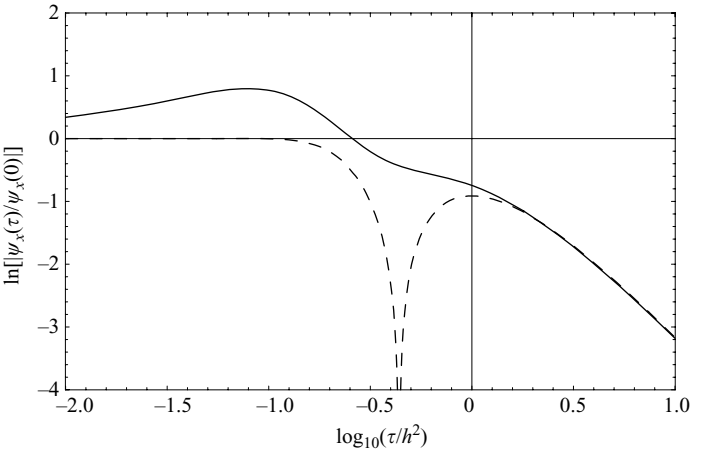


FIGURE 10. Plot of $\ln[|\psi_x(\tau)/\psi_x(0)|]$ for the no-slip boundary condition (solid curve) and for perfect slip boundary condition (dashed curve) as functions of $\log_{10}(\tau/h^2)$.

The behaviour at intermediate times is found easily from (5.17) by numerical integration. In figure 10 we plot $\log[\psi_x(\tau)/\psi_x(0)]$ as a function of $\log_{10}(\tau/h^2)$. The amplitude of the long-time tail in (5.13) and (5.22) is such that the $t^{-3/2}$ long-time tail in the velocity autocorrelation function of a Brownian particle in infinite space is precisely cancelled. Thus the wall has a strong effect on the long-time behaviour. We predicted in particular that the autocorrelation function of the vertical component of velocity decays with a $t^{-5/2}$ long-time tail of negative amplitude. The theoretical predictions have been confirmed by experiment (Jeney *et al.* 2008).

It is of interest to compare with the corresponding relaxation functions for the perfect slip boundary condition. From (2.2) and (5.1) we find

$$\psi_x^{sl}(\tau) = \frac{3}{2\nu} T_{xx}(\boldsymbol{r}_0 - \overline{\boldsymbol{r}}_0, t), \qquad \psi_z^{sl}(\tau) = \frac{-3}{2\nu} T_{zz}(\boldsymbol{r}_0 - \overline{\boldsymbol{r}}_0, t). \tag{5.23}$$

From the explicit expression (2.2) one finds for the first function

$$\psi_x^{sl}(\tau) = \frac{3}{4\sqrt{\pi}}\left(\frac{1}{2h^2\sqrt{\tau}} + \frac{1}{\tau^{3/2}}\right)\mathrm{e}^{-h^2/\tau} - \frac{3}{16h^3}\mathrm{erf}\frac{h}{\sqrt{\tau}}, \tag{5.24}$$

and for the second function

$$\psi_z^{sl}(\tau) = \frac{3}{4h^2\sqrt{\pi\tau}}\mathrm{e}^{-h^2/\tau} - \frac{3}{8h^3}\mathrm{erf}\frac{h}{\sqrt{\tau}}. \tag{5.25}$$

These functions have the same initial values as in (5.12) and (5.21),

$$\psi_x^{sl}(0) = -\frac{3}{16h^3}, \qquad \psi_z^{sl}(0) = -\frac{3}{8h^3}, \tag{5.26}$$

as one would expect. The long-time behaviour is given by

$$\psi_x^{sl}(\tau) \approx \frac{1}{2\sqrt{\pi}}\tau^{-3/2}, \qquad \psi_z^{sl}(\tau) \approx \frac{-1}{2\sqrt{\pi}}\tau^{-3/2}, \qquad \text{as } \tau \to \infty. \tag{5.27}$$

Thus at long times the relaxation function for parallel excitation has the sign opposite that for the no-slip boundary condition. This implies that for perfect slip at the wall the velocity autocorrelation function of a Brownian particle $C_{xx}(t)$ decays with a $t^{-3/2}$

long-time tail rather than with a $t^{-5/2}$ tail. At long times

$$C_{xx}(t) \approx \frac{k_B T}{6\rho[\pi\nu]^{3/2}} t^{-3/2} \qquad \text{as } t \to \infty \qquad \text{(slip)}. \tag{5.28}$$

The amplitude is twice that for infinite space without wall.

In figure 9 we compare the behaviour of $\log[\psi_z(\tau)/\psi_z(0)]$ as a function of $\log_{10}(\tau/h^2)$ for the no-slip boundary condition with that for perfect slip. In figure 10 we make the same comparison for $\log[|\psi_x(\tau)/\psi_x(0)|]$. In this case the normalized relaxation function $\gamma_{xx}^{sl}(\tau) = \psi_x^{sl}(\tau)/\psi_x^{sl}(0)$ for perfect slip passes through zero and decays with a negative $\tau^{-3/2}$ long-time tail.

## 6. Discussion

We have found an efficient way of calculating the flow of a viscous incompressible fluid generated by a sudden impulse near a wall with the no-slip boundary condition. Far from the wall the flow is nearly the same as for the perfect slip boundary condition, but near the wall it is significantly different. For the perfect slip boundary condition the pressure disturbance vanishes immediately after the impulse, but for the no-slip boundary condition there is a space- and time-dependent pressure disturbance. At short times the pressure disturbance is large, and it even diverges in the limit of vanishing time.

Frenkel and co-workers have studied the dynamics of a viscous fluid near a wall with the no-slip boundary condition (Hagen *et al.* 1997) or confined between plane walls (Pagonabarraga *et al.* 1999) and have performed lattice Boltzmann simulations, with particular attention to the long-time tail of the velocity autocorrelation function of a Brownian particle. They have pointed out that the no-slip boundary condition couples the vorticity mode with the pressure. In confined geometry this leads to an over-damped sound mode if the fluid is compressible. Frydel & Rice (2006) have studied the effect of the perfect slip boundary condition.

In earlier works we have studied the velocity autocorrelation function of a Brownian particle immersed in a compressible fluid near a plane wall (Felderhof 2005*c*) or between plane walls (Felderhof 2006). It would be desirable to obtain also the time-dependent Green function for a compressible fluid near a wall or between plane walls, but the analysis becomes more complicated than for the incompressible fluid studied here.

## REFERENCES


Acheson, D. J. 1990 *Elementary Fluid Dynamics*. Clarendon.

Carslaw, H. S. & Jaeger, J. C. 1959 *Conduction of Heat in Solids*. Clarendon.

Cichocki, B. & Felderhof, B. U. 2000 Long-time tails in the solid-body motion of a sphere immersed in a suspension. *Phys. Rev.* E **62**, 5383.

Felderhof, B. U. 2005*a* Effect of the wall on the velocity autocorrelation function and long-time tail of Brownian motion. *J. Phys. Chem.* **109**, 21406.

Felderhof, B. U. 2005*b*. Effect of the wall on the velocity autocorrelation function and long-time tail of Brownian motion: erratum *J. Phys. Chem.* **110**, 13304.

Felderhof, B. U. 2005*c* Effect of the wall on the velocity autocorrelation function and long-time tail of Brownian motion in a viscous compressible fluid. *J. Chem. Phys.* **123**, 184903.

Felderhof, B. U. 2006 Diffusion and velocity relaxation of a Brownian particle immersed in a viscous compressible fluid confined between two parallel plane walls. *J. Chem. Phys.* **124**, 054111.

Felderhof, B. U. 2009 Diffusion and convection after escape from a potential well. *Physica* A **388**, 1388.

Frydel, D. & Rice, S. A. 2006 Lattice-Boltzmann study of the transition from quasi-two-dimensional to three-dimensional one particle hydrodynamics. *Mol. Phys.* **104**, 1283.

Frydel D. & Rice, S. A. 2007 Hydrodynamic description of the long-time tails of the linear and rotational velocity autocorrelation functions of a particle in a confined geometry. *Phys. Rev.* E **76**, 061404.

Hagen, M. H. J., Pagonabarraga, I., Lowe, C. P. & Frenkel, D. 1997 Algebraic decay of velocity fluctuations in a confined fluid. *Phys. Rev. Lett.* **78**, 3785.

Happel, J. & Brenner, H. 1973 *Low Reynolds Number Hydrodynamics*. Noordhoff.

Jeney, S., Lukić, B., Kraus, J. A., Franosch, T. & Forró, L. 2008 Anisotropic memory effects in confined colloidal diffusion. *Phys. Rev. Lett.* **100**, 240604.

Jones, R. B. 1981 Hydrodynamic fluctuation forces. *Physica* A **105**, 395.

Kim, S. & Karrila, S. J. 1991 *Microhydrodynamics: Principles and Selected Applications*. Butterworth-Heinemann.

Kraus, J. A. 2007 Hydrodynamics at micro- and nanoscales. Diploma thesis, University of Munich.

Lighthill, J. 1986 *An Informal Introduction to Theoretical Fluid Mechanics*. Clarendon.

Oseen, C. W. 1927 *Hydrodynamik*. Akademische Verlagsgesellschaft.

Pagonabarraga, I., Hagen, M. H. J., Lowe, C. P. & Frenkel, D. 1998 Algebraic decay of velocity fluctuations near a wall. *Phys. Rev.* E **58**, 7288.

Pagonabarraga, I., Hagen, M. H. J., Lowe, C. P. & Frenkel, D. 1999 Short-time dynamics of colloidal suspensions in confined geometries. *Phys. Rev.* E **59**, 4458.

Pozrikidis, C. 1989 A singularity method for unsteady linearized flow. *Phys. Fluids* A **1**, 1508.

Schlichting, H. 1987 *Boundary Layer Theory*. McGraw-Hill.

Sommerfeld, A. 1909 Über die Ausbreitung der Wellen in der drahtlosen Telegraphie. *Ann. der Phys.* **28**, 665.

Sommerfeld, A. & Renner, F. 1942 Strahlungsenergie und Erdabsorption bei Dipolantennen. *Ann. der Phys.* **41**, 1.